Physics Letters B 834 (2022) 137458

Contents lists available at ScienceDirect

Physics Letters B

www.elsevier.com/locate/physletb

Enhanced moments of inertia for rotation in neutron-rich nuclei

Kenichi Yoshida

Department of Physics, Kyoto University, Kyoto, 606-8502, Japan

ARTICLE INFO

Article history:
Received 5 May 2022
Received in revised form 13 September 2022
Accepted 13 September 2022
Available online 15 September 2022
Editor: J.-P. Blaizot

ABSTRACT

Ground-state moments of inertia (MoI) are investigated for approximately 1700 even–even nuclei from the proton drip line to the neutron drip up to $Z = 120$ and $N = 184$. The cranked Hartree–Fock–Bogoliubov equation is solved in the coordinate space using the Skyrme and pairing energy density functionals. This model well describes the available experimental data of the first excited $I^\pi = 2^+$ state energy of more than 300 nuclides possessing appreciable deformation. The MoI is found to greatly increase near the drip line, whereas the deformation is found to be not as strong as estimated by the empirical relation when the pairing functional including the isovector-density dependence is adopted. The currently used pairing functionals produce large uncertainties in the prediction of $E(2_1^+)$ values near the neutron drip line.

© 2022 The Author. Published by Elsevier B.V. This is an open access article under the CC BY license (http://creativecommons.org/licenses/by/4.0/). Funded by SCOAP[3].

1. Introduction

Nuclear rotational motion occurs in response to the spontaneous breaking of rotational symmetry [1]. With divergence from the magic number, the first excited $I^\pi = 2^+$ state becomes lower in energy: The collective mode of excitation changes character from vibrational to rotational as the deformation develops. A naïve question arises here: How strong should the deformation be for the picture of the rotation to be well-drawn?

Recently, various spectroscopic studies have been carried out to explore unique structures in neutron-rich nuclei. The excitation energy of the 2_1^+ state, $E(2_1^+)$, is often among the first quantities accessible in experiments, and systematic measurements have revealed the evolution of the shell structure [2–4]. In addition to the change of the shell structure associated with the onset of deformation, the $E(2_1^+)$ value may provide rich information about exotic nuclei. A substantial lowering of $E(2_1^+)$ observed in a near-drip-line nucleus ^{40}Mg could be a signal of new physics in drip-line nuclei [5] given that theoretical calculations have predicted that the magnitude of deformation is not enhanced in ^{40}Mg compared with that of Mg isotopes with fewer neutrons [6–13].

The pair correlation is present in the ground state and plays a decisive role in describing various phenomena such as the energy gap in spectra of even–even nuclei and the odd–even staggering in binding energies [14,15]. In addition, the pairing is indispensable for a strong collectivity of the low-frequency quadrupole vibration [16] and a reduced value of moments of inertia (MoI) for rotation compared with the values provided by the rigid-body estimation [14]. Therefore, the $E(2_1^+)$ value should be scrutinized by considering not only the deformation but also the superfluidity.

Another critical issue in exploring the drip-line nuclei is the requirement for careful treatment of the asymptotic part of the nucleonic density. An appropriate framework is the Hartree–Fock–Bogoliubov (HFB) theory solved in the coordinate-space representation [17,18]. This method has been used extensively in describing spherical systems but is much more difficult to implement for systems with deformed equilibrium shapes. Therefore, calculations have been mostly restricted to axially symmetric nuclei [19–24]. A standard technique to describe the nonaxial shape is to employ a truncated single-particle basis, which consists of localized states and discretized-continuum oscillating states, for solutions of the HFB equation [25]. Such a method should not be able to adequately describe the spatial profile of densities at large distances. Recently, the HFB equation has been solved using the contour integral technique and the shifted Krylov subspace method for the Green's function [26,27] to circumvent the successive diagonalization of the matrix with a huge dimension. A canonical-basis method has also been developed [28].

In the present work, I investigate the rotational motion in neutron-rich nuclei near the drip line with emphasis on the pairing. At high spins where the pairing vanishes, a novel mechanism of a nucleus being bound beyond the neutron drip line is proposed [29]. Here, I study the lowest spin state—specifically, the 2_1^+ state—in even–even nonspherical nuclei. A key quantity is the MoI for rotation: $E(2_1^+) = 6/2\mathcal{J}$.

E-mail address: kyoshida@ruby.scphys.kyoto-u.ac.jp.

https://doi.org/10.1016/j.physletb.2022.137458
0370-2693/© 2022 The Author. Published by Elsevier B.V. This is an open access article under the CC BY license (http://creativecommons.org/licenses/by/4.0/). Funded by SCOAP[3].

2. Model and method

The MoI is evaluated microscopically by the Thouless–Valatin procedure or the self-consistent cranking model as $\mathcal{J} = \lim_{\omega_{\rm rot}\to 0}\frac{J_x}{\omega_{\rm rot}}$ where $J_x = \langle \hat{J}_x \rangle$ and $\omega_{\rm rot}$ is the rotational frequency about the x-axis [14]. I solve the cranked HFB (CHFB) equation to obtain the MoI and take the natural units: $\hbar = c = 1$.

The numerical procedure to solve the CHFB equation is described elsewhere [30]. I impose the reflection symmetry about the (x, y)-, (y, z)-, and (z, x)-planes. Thus, the parity $\mathfrak{p}_k$ $(= \pm 1)$ and x-signature r_k $(= \pm \mathrm{i})$ are a good quantum number. I solve the CHFB equation by diagonalizing the HFB Hamiltonian in the three-dimensional (3D) Cartesian mesh representation with the box boundary condition. Because of the reflection symmetries, I have only to consider the octant region explicitly in space with $x \geq 0$, $y \geq 0$, and $z \geq 0$ (see Refs. [31,32] for details). I use a 3D lattice mesh $x_i = ih - h/2$, $y_j = jh - h/2$, $z_k = kh - h/2$ $(i, j, k = 1, 2, \cdots M)$ with a mesh size $h = 1.0$ fm and $M = 12$ for each direction. A reasonable convergence with respect to the mesh spacing h and the box size M is obtained for not only light drip-line nuclei but also medium-mass nuclei [30], although the results contain a numerical error due to severe conditions. In the following, I investigate the numerical error for the case of heavy nuclei, taking ^{250}Fm as an example. I also discuss the weak binding effect by varying M for medium-mass drip-line nuclei.

For diagonalizing the HFB matrix, I use the ScaLAPACK PDSYEV subroutine [33]. A modified Broyden's method [34] is used to calculate new densities during the self-consistent iteration. The quasiparticle energy is cut off at 60 MeV. Each iteration requires ~ 10 core hours at the SQUID computer facility of Osaka University [35]. To achieve convergence, 50–100 iterations using 72 cores/node and 6 nodes (~ 100 node hours) are typically needed. Therefore, the total computational cost for a systematic calculation of 1700 nuclei is $\sim 17,000$ node hours.

3. Results and discussion

3.1. Validity of the present model

The MoI of the ground state is evaluated at $\omega_{\rm rot} = 0.01$ MeV, which is sufficiently low because the lowest $E(2_1^+)$ is ~ 50 keV [36]. I used the SkM* [37] and SLy4 [38] functionals augmented by the Yamagami–Shimizu–Nakatsukasa (YSN) pairing-density functional [39], which is given as

$$\mathcal{E}_{\rm pair}(\boldsymbol{r}) = \frac{V_0}{4}\sum_{\tau={\rm n,p}} g_\tau[\rho,\rho_1]|\tilde{\rho}_\tau(\boldsymbol{r})|^2 \tag{1}$$

with

$$g_\tau[\rho,\rho_1] = 1 - \eta_0\frac{\rho(\boldsymbol{r})}{\rho_0} - \eta_1\frac{\tau_3\rho_1(\boldsymbol{r})}{\rho_0} - \eta_2\left[\frac{\rho_1(\boldsymbol{r})}{\rho_0}\right]^2. \tag{2}$$

Here, $\rho(\boldsymbol{r})$ and $\rho_1(\boldsymbol{r})$ are the isoscalar and isovector densities, respectively; $\tau = $ n (neutron, $\tau_3 = +1$) or p (proton, $\tau_3 = -1$); and $\rho_0 = 0.16$ fm^{-3} is the saturation density of symmetric nuclear matter. The parameters V_0, η_0, η_1, and η_2 were optimized to reproduce the experimental pairing gaps globally and are summarized in Table III of Ref. [39]. Note that the parameters for the ρ_1 dependence η_1, η_2 are positive. The YSN pairing functional was constructed on the basis of the finding that the inclusion of the isospin dependence in the pairing functional gives a good reproduction of the pairing gaps in both stable and neutron-rich nuclei and in both symmetric nuclear matter and neutron matter [40,41].

The multipole moments are introduced as

$$\alpha_{lm} = \frac{4\pi}{3A\bar{R}^l}\int d^3r\, r^l X_{lm}(\hat{r})\rho(\boldsymbol{r}), \tag{3}$$

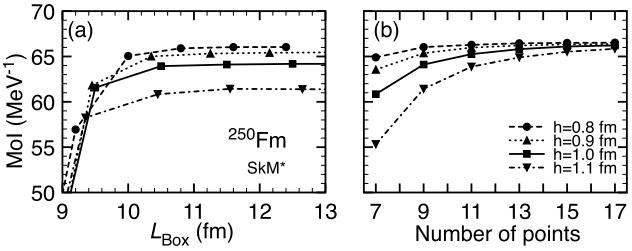

Fig. 1. Calculated moments of inertia $\mathcal{J}$ for ^{250}Fm using the SkM* functional. (a) Dependence on the box size $L_{\rm Box}$ for various mesh spacing h obtained using the 9-point formula: $L_{\rm Box} = (M-1/2)h$. (b) Dependence on the order of approximation for the finite difference method at $L_{\rm Box} \simeq 11.5$ fm. For the case of $h = 0.9$ fm, averaged values obtained with $M = 13$ and 14 are shown.

where $\rho(\boldsymbol{r})$ is the particle density; $\bar{R} = \sqrt{\frac{5}{3A}\int d^3r\, r^2\rho(\boldsymbol{r})}$; and X_{lm} are the real basis of the spherical harmonics. I then define the quadrupole deformation parameter β and the triaxial deformation parameter γ [1] by

$$\alpha_{20} = \beta\cos\gamma, \quad \alpha_{22} = \beta\sin\gamma. \tag{4}$$

Notably, β is positive.

Before investigating the MoI, I examine a numerical error due to the finite h and M adopted in the actual calculations. The box size is given as $L_{\rm Box} = (M-1/2)h$. Fig. 1(a) shows the MoI calculated by changing h and M for ^{250}Fm. For each h, the converged value around $L_{\rm Box}$ =11–12 fm is obtained; this result is consistent with that in Ref. [30]. However, the calculation does not show the convergence with respect to h at a given box size. Using a finer mesh spacing is difficult with the current computational power. I then investigate the order of approximation for the finite difference method. Fig. 1(b) shows the MoI obtained by employing the n-point formula with $n = 7, 9, \ldots 17$. For a smaller mesh size h, better convergence can be obtained with lower-order approximations. The 9-point formula is used in the present analysis; the results are displayed in Fig. 2. These results thus contain ~ 2–3% error in the MoI.

There are 657 even–even nuclei with known $E(2_1^+)$ [36]. In the present study, I limit the scope by excluding the very light nuclei $(Z < 10)$, for which mean-field theory is least justified. This eliminates 22 nuclei. There is no collective rotation in spherical nuclei where the MoI is zero. I defined the spherical nuclei if the calculated MoI is less than 0.1 MeV^{-1}. An additional 273 (260) nuclei are thus eliminated, leaving 362 (375) nuclei in the present analysis using the SkM* (SLy4) functional.

Figs. 3(a) and 3(b) show the calculated MoI obtained using SkM* and SLy4 versus the experimentally obtained values. The experimental data are evaluated as $3/E(2_1^+)$. The points follow the diagonal line reasonably well, with some scatters that vary in extent over the different regimes. For transitional nuclei, one may wonder about the validity of the present model. The filled symbols in Figs. 3(a) and 3(b) denote the weakly deformed nuclei having $\beta < 0.1$. These nuclei give a small value for the MoI, corresponding to $E(2_1^+)$ values greater than the measured values. Furthermore, a distinct deviation from the straight line is observed for the highest region near $\mathcal{J} = 60$ MeV^{-1}: ^{238,240}Cm and ^{244}Cf.

To quantitatively measure the theoretical accuracy, I compare theoretical and experimental results and examine the statistical properties of the quantity $R = \mathcal{J}_{\rm th}/\mathcal{J}_{\rm exp}$. Here, $\mathcal{J}_{\rm th}$ and $\mathcal{J}_{\rm exp}$ are the theoretical and experimental MoI, respectively. A histogram of the distribution of R is shown in Figs. 3(c) and 3(d). For SkM* (SLy4), the average is $\bar{R} = 1.02$ (1.16). When the weakly deformed nuclei with $\beta < 0.1$ are excluded, $\bar{R} = 1.07$ (1.15) for 332 (350) data. Therefore, the present model overestimates the MoI by $\sim 10\%$.

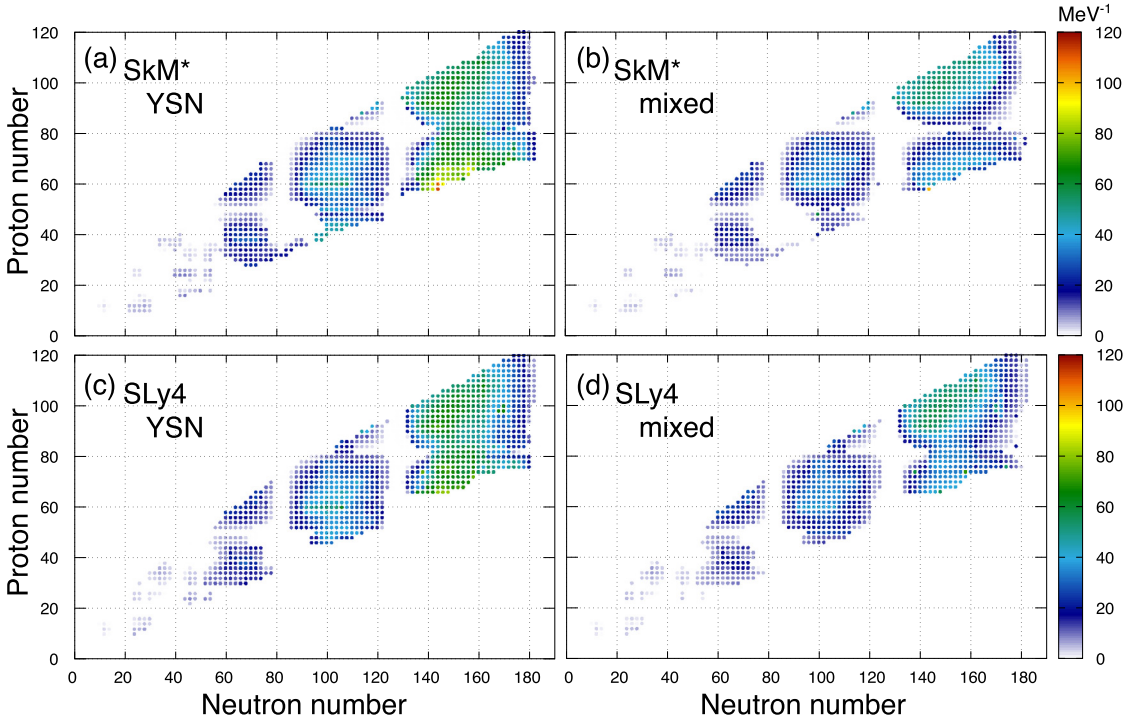

Fig. 2. Calculated moments of inertia $\mathcal{J}$ for the SkM* and SLy4 functionals combined with the pairing functional of the (a,c) YSN and (b,d) mixed types.

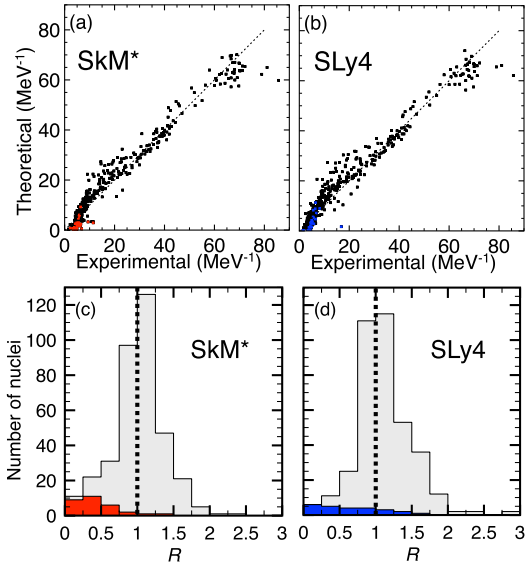

Fig. 3. Calculated MoI for (a) 362 nuclei for the SkM* functional and (b) 375 nuclei for the SLy4 functional, plotted against the corresponding experimental values. Filled symbols indicate 30 (25) nuclei possessing a weak deformation with $\beta < 0.1$ with SkM* (SLy4). Histograms of the quantity $R = \mathcal{J}_{\rm th}/\mathcal{J}_{\rm exp}$ for the (c) SkM* and (d) SLy4 data sets. The dark area indicates nuclei possessing weak deformation with $\beta < 0.1$.

The width of the distribution is an important quantity for determining the accuracy and reliability of the theory. The error is systematic, and the overall distribution is strongly peaked when the weakly deformed nuclei that cause a tail at small R are excluded. The root-mean-square deviation (i.e., the dispersion) of R about its mean is $\sigma = 0.30$ (0.35). Thus, a typical error is approximately 30–35%.

A comparison between the present calculation results and the results of beyond-mean-field-type calculations is interesting [42, 43]. The excited 2^+ states were obtained by the minimization after projection (MAP) and the generator coordinate method (GCM) using the SLy4 functional [42] or the five-dimensional collective Hamiltonian (5DCH) based on the GCM, together with the Gaussian overlap approximation using the Gogny D1S functional [43]. Sabbey et al. [42] and Bertsch et al. [43] introduced the measure $R_E = \ln(E_{\rm th}(2^+)/E_{\rm exp}(2^+))$ to evaluate the validity of the theoretical framework. I then evaluate $E(2^+)$ as $3/\mathcal{J}$ in the present model: $R_E = -0.021(-0.095), \sigma_E = 0.33(0.30)$ for the SkM* (SLy4) functional.

The present model gives a description of the average energy that is similar to that obtained using the 5DCH approach ($R_E = 0.12, \sigma_E = 0.33$ [43]) and is better than the descriptions based on the MAP and GCM models. This comparison indicates that the 2_1^+ state is mostly governed by the rotational MoI of the ground state and that the self-consistent cranking model describes the 2_1^+ state surprisingly well for deformed nuclei with $\beta > 0.1$.

I here briefly describe the performance of the intrinsic quadrupole deformation. For selected nuclei of the Nd and Sm isotopes, the mean-field approximation has been demonstrated to well describe the evolution of deformation (see Fig. 1 of Ref. [44]). There are 396 even–even nuclei with known β [36], where the deformation parameter is evaluated from the $E2$ transition probability: $\beta = (4\pi/3ZR_0^2)\sqrt{B(E2)/e^2}$ [14]. I exclude ten very light nuclei ($Z < 10$). An additional 156 (146) spherical nuclei have been eliminated as in the previously described analysis, leaving 230 (240) nuclei for SkM* (SLy4). The measured $R_\beta = \ln(\beta_{\rm cal}/\beta_{\rm exp})$ is defined similarly as $E(2_1^+)$. I then find $\bar{R}_\beta = -0.12(-0.11)$ with the dispersion $\sigma = 0.35(0.30)$, and $\bar{R}_\beta = -0.08(-0.09)$, $\sigma = 0.26(0.22)$ for 219 (233) nuclei with $\beta > 0.1$. The performance is as good as that of the MoI.

3.2. Moments of inertia of drip-line nuclei

Here, the MoI of neutron-rich nuclei are investigated and unique features near the drip line are discussed. Figs. 2(a) and 2(c) show the MoI calculated using the SkM* and SLy4 functionals, respectively. The even–even nuclei up to $Z = 120$ and those below the magic number of $N = 184$ are included. Striking features

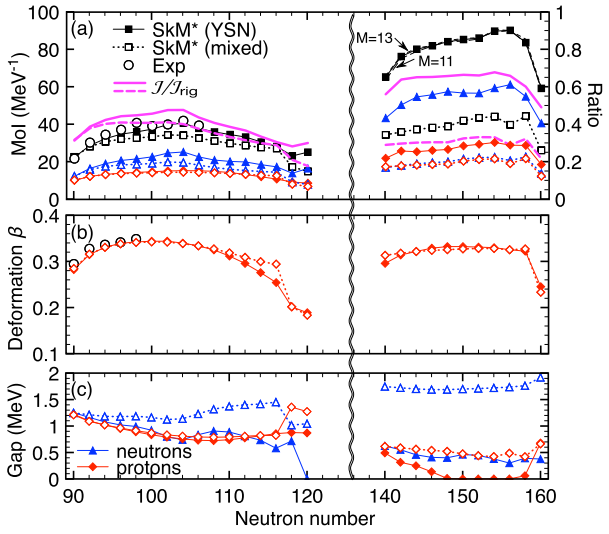

Fig. 4. *Upper*: MoI for the Dy isotopes with $N = 90$–120 and $N = 140$–160. Contributions of neutrons (triangles) and protons (diamonds) are also shown. Ratios $\mathcal{J}/\mathcal{J}_{\rm rig}$ are displayed by lines. The solid (long-dashed) line indicates the results obtained using the YSN (mixed) pairing. *Middle*: Deformation parameters β of protons. *Lower*: Average pairing gaps of neutrons and protons. The filled (open) symbols denote the results obtained using the YSN (mixed) pairing. Calculated values are compared with available experimental data (open circles) [36]. The experimental data for $N = 106$ are taken from Ref. [45].

observed in the result shown in Fig. 2 are that the deformation is strong in the neutron-rich lanthanide nuclei at $N \approx 100$ and that the MoI are accordingly large. In addition, the MoI of the rare-earth nuclei near the drip line are comparable to those of the heavy actinide nuclei even though their mass numbers differ by ~ 40.

I here take neutron-rich Dy isotope as an example of rare-earth nuclei and investigate the mechanism of the enhanced MoI near the drip line in detail. Fig. 4 shows the calculated, MoI together with the deformation parameter β and the pairing gap energy, for $N = 90$–120 and $N = 140$–160, where the pairing gap energy is defined by $\Delta_\tau = \int d\boldsymbol{r}\tilde{h}_\tau(\boldsymbol{r})\tilde{\rho}^*_\tau(\boldsymbol{r})/\int d\boldsymbol{r}\tilde{\rho}^*_\tau(\boldsymbol{r})$. These isotopes are well deformed ($\beta \gtrsim 0.2$), and the estimation of $E(2^+_1)$ is reliable. The experimental data for β are available for N as large as 98, and the present calculation well reproduces the isotopic dependence. The $E(2^+_1)$ value has been measured for N as large as 106 [45]. Although the largest deformation was expected at $N = 100$, the MoI is the largest at $N = 98$ and 104. The calculation also produces the largest MoI at $N = 104$. This result is due to the weakening of the pairing of neutrons: the pairing gap energy of neutrons is the lowest at $N = 104$ among the isotopes with $N = 90$–112, as shown in Fig. 4(c). The increase at $N = 120$ is due to the vanishing pairing gap of neutrons. The value of MoI is sensitively determined by the shell effect and the pairing.

An exotic behavior appears as the drip line is approached. The MoI in the isotopes with $N \sim 150$ is approximately twice as large as that in the $N \sim 100$ region even though the deformation of protons is approximately the same. Because the neutrons are spatially extended, the β of neutrons and that of matter are both smaller than those in the $N \sim 100$ region, which is contrary to a naïve expectation of a large MoI. Fig. 4(a) shows the calculated MoI obtained by changing the box size. The resultant MoI in the very neutron-rich nucleus of ^{226}Dy, whose chemical potential for neutrons is -0.26 MeV, is 58.6 MeV^{-1}, 59.3 MeV^{-1}, and 59.6 MeV^{-1} for $M = 11$, 12, and 13, respectively. The results for $M = 11$, 12, and 13 do not substantially differ, which indicates that the weak binding is not a primal reason for the enhanced MoI. The pairing is a possible origin of this unique feature near the drip line. Notably, the pairing among the continuum states is reasonably described with this box size. The pairing gap of neutrons (protons) in ^{226}Dy is 0.69 MeV (0.39 MeV), 0.68 MeV (0.39 MeV), and 0.67 MeV (0.39 MeV) for $M = 11$, 12, and 13, respectively.

In asymmetric systems, the isovector densities appear to play a role. To observe the effects of the isovector densities in the pairing density functional, I performed the calculation without the ρ_1 terms in Eq. (2); I set the parameters η_1, η_2 to zero while keeping $\eta_0 = 1/2$. These parameters correspond to the mixed volume and surface. I fixed the strength V_0 in Eq. (1) to the pairing gaps of ^{156}Dy for the YSN functional [39]. The strengths $V_0 = -289$ (-326) MeV fm^3 and -324 (-343) MeV fm^3 found for neutrons and protons with SkM* (SLy4) produce the same pairing gaps as those obtained using the YSN functional [see Fig. 4(c)] at $N = 90$. The performance for describing the available $E(2^+)$ is as good as that of the YSN functional. The calculated MoI are displayed in Figs. 2(b) and 2(d) and in Fig. 4(a) for the Dy isotopes. The magnitude of deformation is similar to that calculated with the YSN functional for both the $N \sim 100$ and $N \sim 150$ regions. However, the pairing gaps of neutrons are larger than those with the YSN functional and are substantially enhanced near the drip line. Therefore, the calculated MoI are slightly smaller around $N = 100$, and a 16% reduction is observed at $N = 104$. A deformed-shell effect sensitively affects the MoI when the YSN pairing is used. Near the drip line, the mixed-type pairing gives an almost 50% reduction of the MoI compared with the YSN pairing. Because the pairing of both neutrons and protons is enhanced, the contributions of neutrons and protons to the total MoI are reduced in comparison with the YSN pairing. To demonstrate the effect of pairing, the ratios $\mathcal{J}/\mathcal{J}_{\rm rig}$ are shown in Fig. 4(a). The ratios obtained with the mixed pairing are slightly smaller than those obtained with the YSN pairing in the $N \sim 100$ region, whereas they decrease in the case of the mixed pairing and increase in the case of the YSN pairing in the $N \sim 150$ region.

The substantial enhancement of the MoI near the drip line when the YSN functional is used is attributed to a deformed-shell effect and to isovector-density dependence (i.e., an effective decrease in the strength) of the pairing functional. Indeed, this mechanism explains the lowering of $E(2^+_1)$ in ^{40}Mg [30]. The reduction in the strength of the pair interaction with increasing asymmetry can be observed by comparing Figs. 5(a) and 5(b). A reduction of the MoI relative to the rigid body is due to the pairing, and the reduction observed in very neutron-rich nuclei with the asymmetry $\alpha = (N - Z)/A > 0.3$ is apparently weakened when the YSN pairing functional is used. Scattering of the data points is associated with the shell effect.

Finally, I discuss the enhancement of the MoI from a different perspective. As the quadrupole collectivity increases, lower energies and stronger transitions are observed. Empirically, the following relation has been found and 91% of the observed 328 data points are reproduced within a factor of two [46]:

$$\left[\frac{B(E2;0^+_1\to 2^+_1)}{1\,e^2\mathrm{fm}^4}\right]\times\left[\frac{E(2^+_1)}{1\,\mathrm{MeV}}\right]=32.6\frac{Z^2}{A^{0.69}}. \tag{5}$$

This equation corresponds to

$$\mathcal{J}=\frac{3}{32.6}\left(\frac{3}{4\pi}\right)^2 A^{0.69}R_0^4\beta^2\ [\mathrm{MeV}^{-1}], \tag{6}$$

where R_0 is expressed in femtometers. Figs. 5(c) and 5(d) show the calculated MoI divided by $A^{2.02}$ and plotted as a function of the deformation parameter β. With the mixed-type pairing, the calculated MoI scatter around the empirical line; most of them are within a factor of two. However, with the YSN functional, the empirical line does not coincide with the trend of the calculated MoI for $\alpha > 0.3$. Therefore, $E(2^+_1)$ can be low in neutron-rich nuclei despite the $B(E2)$ value not being high. Although the currently used

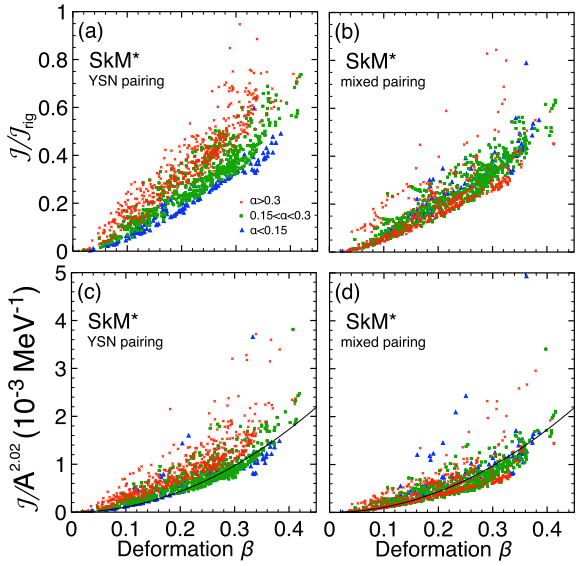

Fig. 5. Ratio between the MoI calculated using the (a) YSN and (b) mixed-type pairing functionals and the MoI for the rigid body. The MoI calculated using the (c) YSN and (d) mixed-type pairing functionals, divided by $A^{2.02}$ are plotted as a function of the deformation parameter β. The line represents Eq. (6) with the approximation $R_0 = 1.2A^{1/3}$ fm. Symbols with a red cross, green square, and blue triangle indicate the asymmetry parameter $\alpha = (N-Z)/A \geq 0.3$, $0.15 \leq \alpha < 0.3$, and $\alpha < 0.15$, respectively.

pairing functionals give a satisfactory description of the available experimental data, they result in a large variation near the drip line.

4. Summary

I carried out systematic calculations of the MoI from the proton drip line to the neutron drip line to elucidate the roles of neutron excess in the collective rotational motion. To describe neutron-rich nuclei in which loosely bound neutrons and the continuum coupling should be considered, I solved the cranked HFB equation in the coordinate space. A comparison with the available experimental data and other models shows that the present model surprisingly well describes the ground-state MoI—specifically, the $E(2_1^+)$ value—for deformed nuclei with $\beta > 0.1$. By using the pairing density functional constructed to describe the isospin dependence in neutron-rich nuclei, I found that the MoI are greatly enhanced near the drip line, whereas the magnitude of deformation is not as strong as estimated by the empirical relation between the $E(2_1^+)$ and $B(E2)$ values. The pairing functional including only the isoscalar density produces the enhanced pairing and reduced MoI relative to the rigid-body value. The currently used pairing functionals give a fair description of the available experimental data of $E(2_1^+)$ with similar accuracy. However, they produce a considerable variation near the drip line.

Declaration of competing interest

The authors declare the following financial interests/personal relationships which may be considered as potential competing interests:

Kenichi Yoshida reports financial support was provided by Japan Society for the Promotion of Science.

Data availability

Data will be made available on request.

Acknowledgements

This work was supported by the JSPS KAKENHI (Grants No. JP19K03824 and No. JP19K03872). The numerical calculations were performed at the computing facilities at the Yukawa Institute for Theoretical Physics, Kyoto University, at the Research Center for Nuclear Physics, Osaka University, and at the Cybermedia Center, Osaka University.

References

[1] A. Bohr, B. Mottelson, Nuclear Structure: Volume II, Nuclear Deformations, Benjamin, Reading, MA, 1975, https://books.google.co.jp/books?id=dRhRAAAAMAAJ.

[2] Shell evolution and search for two-plus energies at RIBF: SEASTAR project, https://www.nishina.riken.jp/collaboration/SUNFLOWER/experiment/seastar/index.php.

[3] A. Gade, Excitation energies in neutron-rich rare isotopes as indicators of changing shell structure, Eur. Phys. J. A 51 (9) (2015) 118, https://doi.org/10.1140/epja/i2015-15118-8.

[4] T. Otsuka, A. Gade, O. Sorlin, T. Suzuki, Y. Utsuno, Evolution of shell structure in exotic nuclei, Rev. Mod. Phys. 92 (2020) 015002, https://doi.org/10.1103/RevModPhys.92.015002.

[5] H.L. Crawford, P. Fallon, A.O. Macchiavelli, P. Doornenbal, N. Aoi, F. Browne, C.M. Campbell, S. Chen, R.M. Clark, M.L. Cortés, M. Cromaz, E. Ideguchi, M.D. Jones, R. Kanungo, M. MacCormick, S. Momiyama, I. Murray, M. Niikura, S. Paschalis, M. Petri, H. Sakurai, M. Salathe, P. Schrock, D. Steppenbeck, S. Takeuchi, Y.K. Tanaka, R. Taniuchi, H. Wang, K. Wimmer, First spectroscopy of the near dripline nucleus ^{40}Mg, Phys. Rev. Lett. 122 (2019) 052501, https://doi.org/10.1103/PhysRevLett.122.052501.

[6] J. Terasaki, H. Flocard, P.-H. Heenen, P. Bonche, Deformation of nuclei close to the two-neutron drip line in the Mg region, Nucl. Phys. A 621 (3) (1997) 706–718, https://doi.org/10.1016/S0375-9474(97)00183-8.

[7] R. Rodríguez-Guzmán, J. Egido, L. Robledo, Correlations beyond the mean field in magnesium isotopes: angular momentum projection and configuration mixing, Nucl. Phys. A 709 (1) (2002) 201–235, https://doi.org/10.1016/S0375-9474(02)01019-9.

[8] K. Yoshida, Skyrme-QRPA calculations for low-lying excitation modes in deformed neutron-rich nuclei, Eur. Phys. J. A 42 (2009) 583–590, https://doi.org/10.1140/epja/i2008-10742-y, arXiv:0902.3053.

[9] K. Yoshida, Collective modes of excitation in deformed neutron-rich Mg isotopes, Mod. Phys. Lett. A 25 (2010) 1783–1786, https://doi.org/10.1142/S0217732310000320.

[10] J.M. Yao, H. Mei, H. Chen, J. Meng, P. Ring, D. Vretenar, Configuration mixing of angular-momentum projected triaxial relativistic mean-field wave functions. II. Microscopic analysis of low-lying states in magnesium isotopes, Phys. Rev. C 83 (2011) 014308, https://doi.org/10.1103/PhysRevC.83.014308, arXiv:1006.1400.

[11] S. Watanabe, K. Minomo, M. Shimada, S. Tagami, M. Kimura, M. Takechi, M. Fukuda, D. Nishimura, T. Suzuki, T. Matsumoto, Y.R. Shimizu, M. Yahiro, Ground-state properties of neutron-rich Mg isotopes, Phys. Rev. C 89 (2014) 044610, https://doi.org/10.1103/PhysRevC.89.044610, arXiv:1404.2373.

[12] T.R. Rodríguez, Precise description of nuclear spectra with Gogny energy density functional methods, Eur. Phys. J. A 52 (7) (2016) 190, https://doi.org/10.1140/epja/i2016-16190-2.

[13] M. Shimada, S. Watanabe, S. Tagami, T. Matsumoto, Y.R. Shimizu, M. Yahiro, Simultaneous analysis of matter radii, transition probabilities, and excitation energies of Mg isotopes by angular-momentum-projected configuration-mixing calculations, Phys. Rev. C 93 (6) (2016) 064314, https://doi.org/10.1103/PhysRevC.93.064314, arXiv:1605.08585.

[14] P. Ring, P. Schuck, The Nuclear Many-Body Problem, Springer-Verlag, New York, 1980.

[15] D.M. Brink, R.A. Broglia, Nuclear Superfluidity: Pairing in Finite Systems, Cambridge Monographs on Particle Physics, Nuclear Physics and Cosmology, Cambridge University Press, 2005.

[16] K. Matsuyanagi, N. Hinohara, K. Sato, BCS-pairing and nuclear vibrations, Fifty Years of Nuclear BCS (2013) 111–124, https://doi.org/10.1142/9789814412490_0009, arXiv:1205.0078.

[17] A. Bulgac, Hartree-Fock-Bogolyubov approximation for finite systems, arXiv:nucl-th/9907088, 8 1980.

[18] J. Dobaczewski, H. Flocard, J. Treiner, Hartree-Fock-Bogolyubov description of nuclei near the neutron-drip line, Nucl. Phys. A 422 (1) (1984) 103–139, https://doi.org/10.1016/0375-9474(84)90433-0.

[19] E. Terán, V.E. Oberacker, A.S. Umar, Axially symmetric Hartree-Fock-Bogoliubov calculations for nuclei near the drip lines, Phys. Rev. C 67 (2003) 064314, https://doi.org/10.1103/PhysRevC.67.064314.

[20] A. Blazkiewicz, V.E. Oberacker, A.S. Umar, M. Stoitsov, Coordinate space Hartree-Fock-Bogoliubov calculations for the zirconium isotope chain up to the two-neutron drip line, Phys. Rev. C 71 (2005) 054321, https://doi.org/10.1103/PhysRevC.71.054321.
[21] K. Yoshida, N. Van Giai, Low-lying dipole resonance in neutron-rich Ne isotopes, Phys. Rev. C 78 (2008) 014305, https://doi.org/10.1103/PhysRevC.78.014305.
[22] H. Oba, M. Matsuo, Deformation around neutron-rich Cr isotopes in axially symmetric Skyrme-Hatree-Fock-Bogoliubov method, Prog. Theor. Phys. 120 (1) (2008) 143–157, https://doi.org/10.1143/PTP.120.143, https://academic.oup.com/ptp/article-pdf/120/1/143/19572180/120-1-143.pdf.
[23] J.C. Pei, M.V. Stoitsov, G.I. Fann, W. Nazarewicz, N. Schunck, F.R. Xu, Deformed coordinate-space Hartree-Fock-Bogoliubov approach to weakly bound nuclei and large deformations, Phys. Rev. C 78 (2008) 064306, https://doi.org/10.1103/PhysRevC.78.064306.
[24] H. Kasuya, K. Yoshida, Hartree-Fock-Bogoliubov theory for odd-mass nuclei with a time-odd constraint and application to deformed halo nuclei, PTEP 2021 (1) (2021) 013D01, https://doi.org/10.1093/ptep/ptaa163, arXiv:2005.03276.
[25] J. Terasaki, P.-H. Heenen, H. Flocard, P. Bonche, 3D solution of Hartree-Fock-Bogoliubov equations for drip-line nuclei, Nuclear Physics A 600 (3) (1996) 371–386, https://doi.org/10.1016/0375-9474(96)00036-X.
[26] S. Jin, A. Bulgac, K. Roche, G. Wlazłowski, Coordinate-space solver for superfluid many-fermion systems with the shifted conjugate-orthogonal conjugate-gradient method, Phys. Rev. C 95 (4) (2017) 044302, https://doi.org/10.1103/PhysRevC.95.044302, arXiv:1608.03711.
[27] Y. Kashiwaba, T. Nakatsukasa, Coordinate-space solver for finite-temperature Hartree-Fock-Bogoliubov calculations using the shifted Krylov method, Phys. Rev. C 101 (4) (2020) 045804, https://doi.org/10.1103/PhysRevC.101.045804, arXiv:2001.00500.
[28] M. Chen, T. Li, B. Schuetrumpf, P.-G. Reinhard, W. Nazarewicz, Three-dimensional Skyrme Hartree-Fock-Bogoliubov solver in coordinate-space representation, Comput. Phys. Commun. 276 (2022) 108344, https://doi.org/10.1016/j.cpc.2022.108344, arXiv:2111.02485.
[29] A.V. Afanasjev, N. Itagaki, D. Ray, Rotational excitations in near neutron-drip line nuclei: the birth and death of particle-bound rotational bands and the extension of nuclear landscape beyond spin zero neutron drip line, Phys. Lett. B 794 (2019) 7–13, https://doi.org/10.1016/j.physletb.2019.05.021, arXiv:1905.11500.
[30] K. Yoshida, Cranked Skyrme-Hartree-Fock-Bogoliubov approach for a mean-field description of nuclear rotations near the drip line, Phys. Rev. C 105 (2) (2022) 024313, https://doi.org/10.1103/PhysRevC.105.024313, arXiv:2109.08328.
[31] P. Bonche, H. Flocard, P. Heenen, Self-consistent calculation of nuclear rotations: the complete yrast line of ^{24}Mg, Nucl. Phys. A 467 (1) (1987) 115–135, https://doi.org/10.1016/0375-9474(87)90331-9.
[32] H. Ogasawara, K. Yoshida, M. Yamagami, S. Mizutori, K. Matsuyanagi, Rotational frequency dependence of octupole vibrations on superdeformed states in ^{40}Ca, Prog. Theor. Phys. 121 (2) (2009) 357–374, https://doi.org/10.1143/PTP.121.357.
[33] ScaLAPACK—scalable linear algebra PACKage, http://www.netlib.org/scalapack/.
[34] A. Baran, A. Bulgac, M.M. Forbes, G. Hagen, W. Nazarewicz, N. Schunck, M.V. Stoitsov, Broyden's method in nuclear structure calculations, Phys. Rev. C 78 (2008) 014318, https://doi.org/10.1103/PhysRevC.78.014318.
[35] SQUID—Supercomputer for Quest to Unsolved Interdisciplinary Datascience, http://www.hpc.cmc.osaka-u.ac.jp/en/squid/.
[36] National Nuclear Data Center, Evaluated nuclear structure data file, https://www.nndc.bnl.gov/ensdf/.
[37] J. Bartel, P. Quentin, M. Brack, C. Guet, H.-B. Håkansson, Towards a better parametrisation of Skyrme-like effective forces: a critical study of the SkM force, Nucl. Phys. A 386 (1) (1982) 79–100, https://doi.org/10.1016/0375-9474(82)90403-1.
[38] E. Chabanat, P. Bonche, P. Haensel, J. Meyer, R. Schaeffer, A Skyrme parametrization from subnuclear to neutron star densities. 2. Nuclei far from stabilities, Nucl. Phys. A 635 (1998) 231–256, https://doi.org/10.1016/S0375-9474(98)00180-8; Erratum: Nucl. Phys. A 643 (1998) 441.
[39] M. Yamagami, Y.R. Shimizu, T. Nakatsukasa, Optimal pair density functional for description of nuclei with large neutron excess, Phys. Rev. C 80 (2009) 064301, https://doi.org/10.1103/PhysRevC.80.064301, arXiv:0812.3197.
[40] J. Margueron, H. Sagawa, K. Hagino, BCS-BEC crossover of neutron pairs in symmetric and asymmetric nuclear matters, Phys. Rev. C 76 (2007) 064316, https://doi.org/10.1103/PhysRevC.76.064316, arXiv:0710.4241.
[41] J. Margueron, H. Sagawa, K. Hagino, Effective pairing interactions with isospin density dependence, Phys. Rev. C 77 (2008) 054309, https://doi.org/10.1103/PhysRevC.77.054309, arXiv:0712.3644.
[42] B. Sabbey, M. Bender, G.F. Bertsch, P.-H. Heenen, Global study of the spectroscopic properties of the first 2^+ state in even-even nuclei, Phys. Rev. C 75 (2007) 044305, https://doi.org/10.1103/PhysRevC.75.044305.
[43] G.F. Bertsch, M. Girod, S. Hilaire, J.-P. Delaroche, H. Goutte, S. Péru, Systematics of the first 2^+ excitation with the Gogny interaction, Phys. Rev. Lett. 99 (2007) 032502, https://doi.org/10.1103/PhysRevLett.99.032502.
[44] K. Yoshida, T. Nakatsukasa, Dipole responses in Nd and Sm isotopes with shape transitions, Phys. Rev. C 83 (2011) 021304, https://doi.org/10.1103/PhysRevC.83.021304, arXiv:1008.1520.
[45] H. Watanabe, et al., Long-lived K isomer and enhanced γ vibration in the neutron-rich nucleus ^{172}Dy: collectivity beyond double midshell, Phys. Lett. B 760 (2016) 641–646, https://doi.org/10.1016/j.physletb.2016.07.057.
[46] S. Raman, C. Nestor, P. Tikkanen, Transition probability from the ground to the first-excited 2+ state of even–even nuclides, At. Data Nucl. Data Tables 78 (1) (2001) 1–128, https://doi.org/10.1006/adnd.2001.0858.